

Supporting information

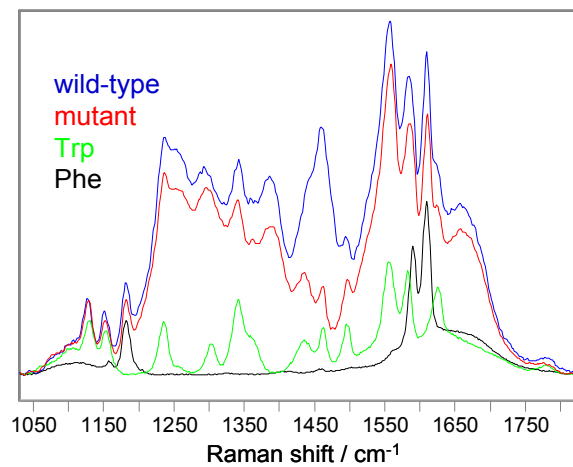


Figure S1. 204-nm excited UVRR spectra of the p53 wild-type peptide, the mutant peptide, tryptophan and phenylalanine at 30°C.

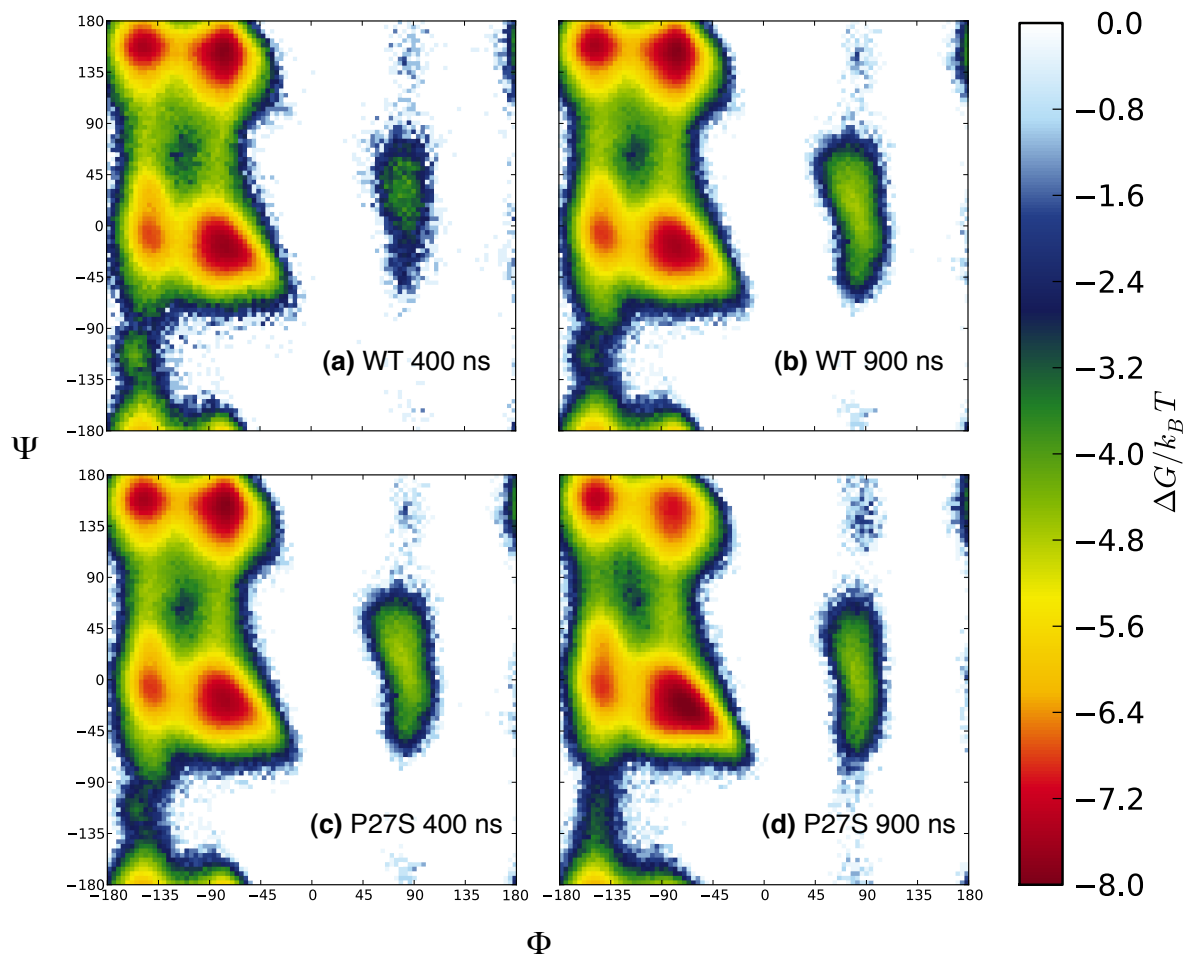


Figure S2. Convergence of simulation ensembles by Ramachandran analysis. After discarding the initial 100 ns of each 1- μ s production run started from different structures, slightly less than half (400 ns) of the remaining structures from each simulation were pooled and used to generate Ramachandran plots for the wild-type and P27S peptides; these were compared to Ramachandran plots containing the entire ensemble of structures (900 ns per initial structure). The distribution of conformations in the wild-type peptide simulation ensemble did not change appreciably when considering 400 ns of data [(a), 45,000 conformations] and when considering 900 ns of data [(b), 90,000 conformations]. Likewise, the distribution of P27S conformations did not change appreciably between 400 ns (c) and 900 ns (d) of production simulation

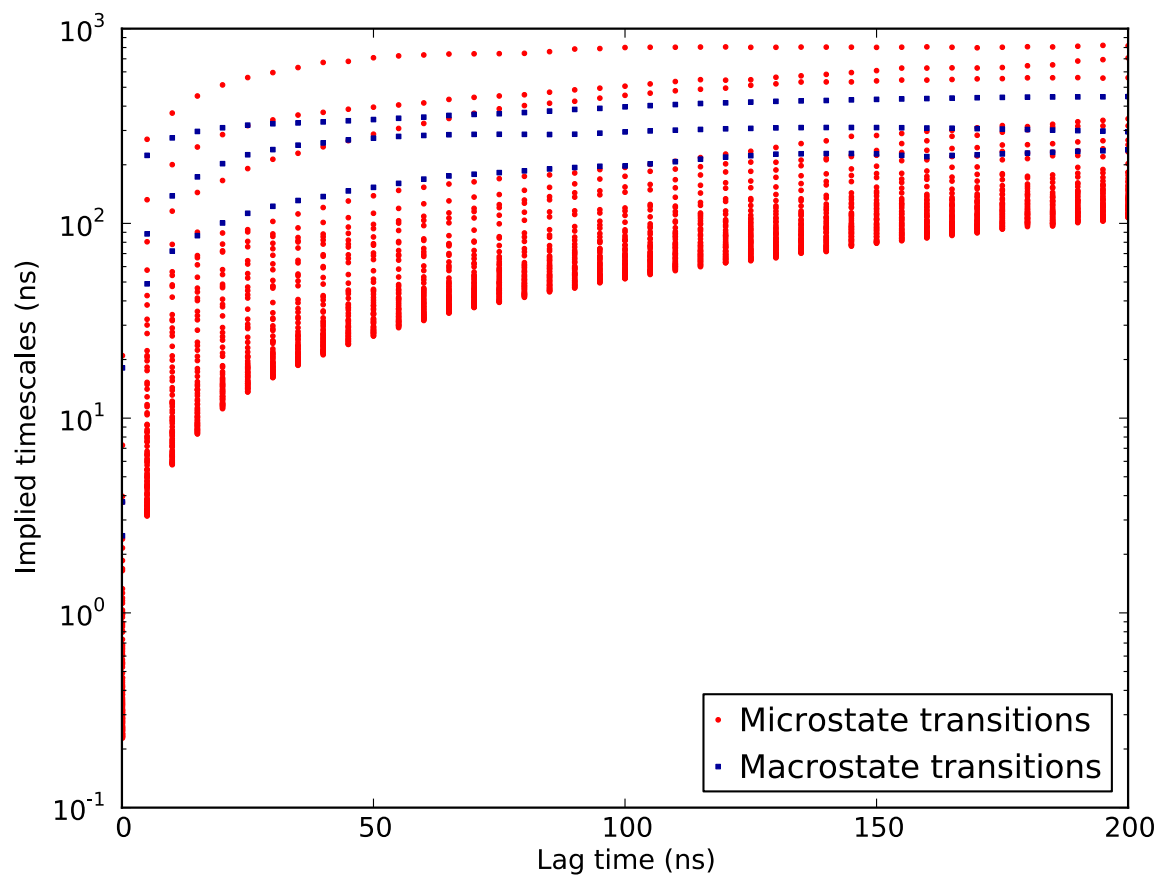


Figure S3. Markovian behavior of the kinetic clustering of wild-type peptide configurations is demonstrated by the invariance of the “implied timescales” (related to the eigenvalues of the transition matrix) beyond a certain timescale (the Markov time of the system). Both the implied timescales of the microstate transition matrix (red circles) and those of the macrostate transition matrix (blue squares) are nearly constant after 50 ns.

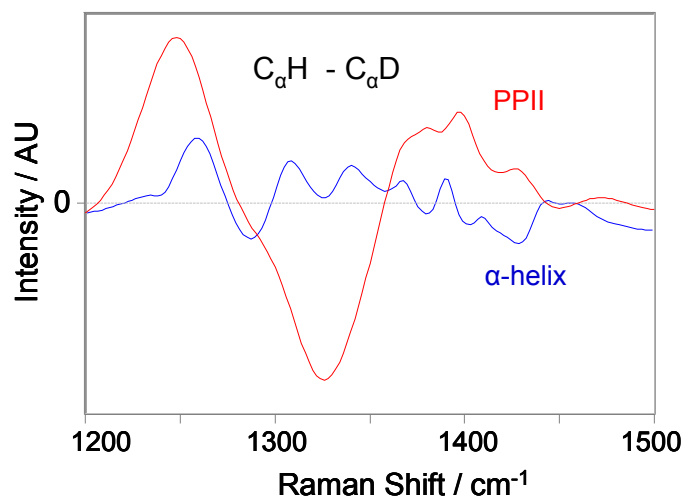


Figure S4. 204-nm UVR difference spectra for the PPII (red) and α -helical conformations (blue) between hydrogenated ($C_{\alpha}H$) versus deuterated ($C_{\alpha}D$) of a mainly polyalanine peptide. UVR spectra of the PPII and α -helical conformations are taken from Fig. 3A of ref 1.¹

Table S1. Comparison of amide and α -proton chemical shifts (HN and HA, respectively) computed from simulations with experimentally measured values² for the wild-type p53 peptide.

Residue	HN chemical shift (ppm)				HA chemical shift (ppm)				
	Simulation	Experiment	RMSD	Relative RMSD	Simulation	Experiment	RMSD	Relative RMSD	
Glu17	8.38	8.39	0.07	0.008	4.22	4.26	0.21	0.049	
Thr18	8.38	8.22	0.50	0.061	4.04	4.28	0.49	0.115	
Phe19	7.95	8.31	0.82	0.099	4.71	4.61	0.50	0.109	
Ser20	8.13	8.14	0.78	0.095	4.34	4.34	0.48	0.111	
Asp21	8.01	8.30	0.64	0.077	4.57	4.56	0.27	0.060	
Leu22	7.95	7.97	0.56	0.071	4.26	4.11	0.32	0.079	
Trp23	7.97	7.87	0.62	0.078	4.79	4.54	0.47	0.103	
Lys24	7.72	7.60	0.61	0.080	4.34	4.07	0.43	0.106	
Leu25	8.00	7.86	0.54	0.069	4.29	4.29	0.36	0.084	
Leu26	7.60	7.98	0.56	0.070	4.40	4.63	0.36	0.077	
Pro27	—	—	—	—	4.46	4.38	0.27	0.063	
Glu28	8.41	8.79	0.57	0.064	4.43	4.21	0.35	0.084	
Asn29	8.59	8.33	0.48	0.058	4.53	4.71	0.25	0.053	
Average:			0.56	0.069	Average:			0.37	0.084

Table S2. Comparison of amide and α -proton chemical shifts (HN and HA, respectively) computed from simulations with experimentally measured values² for the P27S mutant p53 peptide.

Residue	HN chemical shift (ppm)				HA chemical shift (ppm)				
	Simulation	Experiment	RMSD	Relative RMSD	Simulation	Experiment	RMSD	Relative RMSD	
Glu17	8.37	8.41	0.08	0.009	4.16	4.27	0.30	0.070	
Thr18	8.32	8.22	0.49	0.059	3.90	4.28	0.66	0.155	
Phe19	7.87	8.33	0.87	0.104	4.70	4.58	0.41	0.089	
Ser20	8.01	8.17	0.71	0.087	4.29	4.34	0.50	0.116	
Asp21	8.10	8.30	0.63	0.076	4.50	4.56	0.25	0.055	
Leu22	7.87	8.00	0.53	0.066	4.28	4.10	0.32	0.079	
Trp23	8.17	7.95	0.58	0.073	4.59	4.46	0.44	0.099	
Lys24	7.85	7.67	0.57	0.075	4.13	3.99	0.36	0.091	
Leu25	7.81	7.82	0.47	0.060	4.31	4.22	0.31	0.073	
Leu26	7.70	8.01	0.68	0.085	4.35	4.29	0.32	0.074	
Ser27	7.81	8.06	0.62	0.077	4.38	4.34	0.35	0.081	
Glu28	8.03	8.31	0.57	0.068	4.45	4.28	0.34	0.078	
Asn29	8.63	8.27	0.56	0.068	4.51	4.69	0.27	0.058	
Average:			0.57	0.070	Average:			0.37	0.086

Table S3. Comparison of $^3J_{\alpha N}$ coupling constants computed from simulations with experimentally measured values² for the wild-type p53 peptide.

Residue	Simulation	Experiment	RMSD	Relative RMSD
Glu17	7.7	6.4	2.0	0.31
Thr18	6.6	7.9	2.6	0.33
Phe19	7.6	—	—	—
Ser20	7.3	5.7	2.6	0.45
Asp21	6.9	6.8	2.2	0.32
Leu22	6.5	—	—	—
Trp23	7.4	—	—	—
Lys24	7.5	—	—	—
Leu25	7.6	—	—	—
Leu26	7.3	—	—	—
Pro27	5.8	—	—	—
Glu28	7.6	5.5	2.8	0.50
Asn29	8.4	—	—	—
Average:			2.4	0.38

Table S4. Comparison of $^3J_{\alpha N}$ coupling constants computed from simulations with experimentally measured values² for the P27S mutant p53 peptide.

Residue	Simulation	Experiment	RMSD	Relative RMSD
Glu17	7.6	6.4	2.0	0.31
Thr18	6.3	7.9	2.8	0.35
Phe19	7.5	6.4	2.2	0.35
Ser20	6.5	5.7	2.7	0.47
Asp21	6.1	—	—	—
Leu22	6.7	5.7	2.2	0.38
Trp23	6.0	5.0	2.4	0.49
Lys24	6.1	5.7	2.1	0.37
Leu25	7.5	6.1	2.1	0.35
Leu26	7.7	5.7	2.6	0.46
Ser27	7.6	6.1	2.3	0.38
Glu28	7.5	—	—	—
Asn29	8.3	7.5	1.5	0.20
Average:			2.3	0.37

Data S1. Ramachandran Ψ angle distribution for the wild-type p53 peptide fragment obtained by UVRR spectroscopy.

Data S2. Ramachandran Ψ angle distribution for the P27S mutant p53 peptide fragment obtained by UVRR spectroscopy.

Data S3. Ramachandran Ψ angle distribution for the wild-type p53 peptide fragment obtained from all-atom molecular dynamics simulations.

Data S4. Ramachandran Ψ angle distribution for the P27S mutant p53 peptide fragment obtained from all-atom molecular dynamics simulations.

1. Ψ -angle distribution for the wild-type p53 peptide

UVRR spectrum decomposition. We used Grams Suite (Version 8.0, Thermo Fisher Scientific, Inc. Waltham, Mass., USA) to model the UVRR spectrum as the sum of Gaussians.³ We constrained the AmIII_3 band widths to be $< 50 \text{ cm}^{-1}$. The AmIII_3 region shown in Fig. S5 was fitted to four Gaussians. This resulted in a fitted $\text{AmIII}_3^{\text{Ta}}$ band at 1206 cm^{-1} , an $\text{AmIII}_3^{\text{PPII}}$ band at 1246 cm^{-1} , an $\text{AmIII}_3^{\text{Tc}}$ band at 1272 cm^{-1} and an $\text{AmIII}_3^{\text{Td}}$ band at 1290 cm^{-1} (Ta, Tc, and Td refer to different types of turns: Type I' or Type III' β turns, γ -turns, and Type V β -turns, respectively). Attempts to fit the AmIII_3 region by using only three Gaussians resulted in large residuals (Fig. S6).

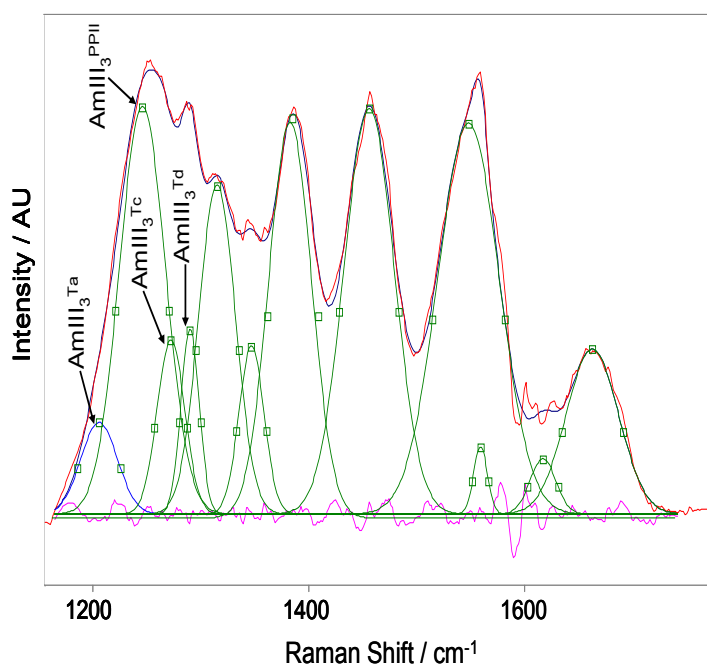


Figure S5. Deconvolution of 204 nm UVRR spectrum of the wild-type peptide at $30 \text{ }^{\circ}\text{C}$. Fit statistics: reduced $\chi^2 = 2.242$; $R^2=0.9925$; standard error= 57.2763.

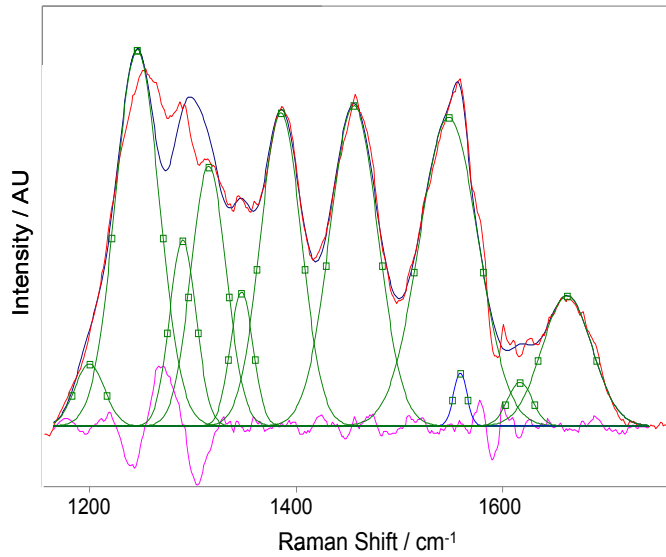


Figure S6. Deconvolution of the AmIII₃ region of the wild-type peptide as the sum of three Gaussians. Fit statistics: reduced $\chi^2 = 12.172$; $R^2 = 1.0151$; standard error = 137.1674.

AmIII₃ band deconvolution. We assume that the inhomogeneously broadened experimentally measured AmIII₃ band profile derives from different conformations and can be modeled by the sum of Lorentzian bands.⁴ We deconvoluted each of the AmIII₃ Gaussians from the Fig. S5 fit into the sum of Lorentzian bands with the homogeneous line widths Γ with different center frequencies νe_i :

$$A(\nu) = \pi^{-1} \sum_{i=1}^M L_i \cdot \frac{\Gamma^2}{\Gamma^2 + (\nu - \nu e_i)^2} \quad (1)$$

where L_i is the probability for a band to occur at frequency νe_i .

Quantitative correlation between the Ψ -angle and AmIII₃ frequency. Equations have been derived correlating the Ψ angle with the AmIII₃ frequency,⁵⁻⁷ thus allowing us to calculate the Ψ -angle distributions.^{4,6} The Ψ -angle distribution for PPII-like conformations was calculated using the following expression derived for peptide bonds fully exposed to solvent:

$$\nu_{AmIII_3}(\Psi, t) = 1256 \text{ cm}^{-1} - 54 \text{ cm}^{-1} \cdot \sin(\Psi + 26^\circ) - 0.11 \frac{\text{cm}^{-1}}{^\circ\text{C}} t \quad (2)$$

The Ψ -angle distribution for Type V β -turns (Td) was calculated by using the following expression derived for peptide bonds⁸ forming two-end-on peptide bond-peptide bond hydrogen bonds.⁵

$$\nu_{AmIII_3}(\Psi) = 1244cm^{-1} - 54cm^{-1} \cdot \sin(\Psi + 26^\circ) \quad (3)$$

The Ψ -angle distributions for Type I' or Type III' β turns (Ta) and γ -turns (Tc) were calculated by using the average expression derived for peptide bonds with unknown hydrogen bonding patterns in aqueous solution:⁵

$$\nu_{AmIII_3}(\Psi, t) = 1250cm^{-1} - 54cm^{-1} \cdot \sin(\Psi + 26^\circ) - 0.06 \frac{cm^{-1}}{^\circ C} t \quad (4)$$

2. Ψ -angle distribution for the P27S mutant p53 peptide

Calculation of non-PPII content. The wild-type p53 peptide has 12 non-proline peptide bonds contributing to Raman intensities in the AmIII, C $_{\alpha}$ -H and AmII regions (athe pro peptide bond shows little intensities in these regions.)⁹ The mutant peptide has 13 non-proline peptide bonds contributing. To normalize to the non-pro peptide bond concentration, we scaled the wild-type peptide spectrum by 13/12. To calculate the fractional increase in non-PPII conformations of the mutant p53 peptide per peptide bond, we subtracted appropriate amounts of the scaled UVRR spectrum of the wild-type peptide from the UVRR spectrum of the mutant peptide to minimize the C $_{\alpha}$ -H region intensity in the difference spectra, with the constraint that no negative features occur. Since the relative spectral intensity subtracted is directly proportional to the population of PPII-like conformations at each temperature, the difference spectra represent only non-PPII conformations.^{10,11} Based on these difference spectra, the population of non-PPII conformations for the mutant peptide was calculated to be ~ 0.6 at all temperatures.

Decomposition of the non-PPII part of the spectrum. We modeled the *AmIII₃* region of the non-PPII part of the spectrum for the mutant peptide as the sum of three Gaussians (Fig. S7). By using the same methodology above, we calculated the Ψ -angle distribution for Type V β -turns by using Eqn. 4, and for α -helix and π -bulge by using Eqn. 3. The overall Ψ -angle distribution contains contributions from α -helix-like conformations, PPII, type V β -turns, Type I' or Type III' β turns, γ -turns, and Type I/I' or Type II/II' β turns.

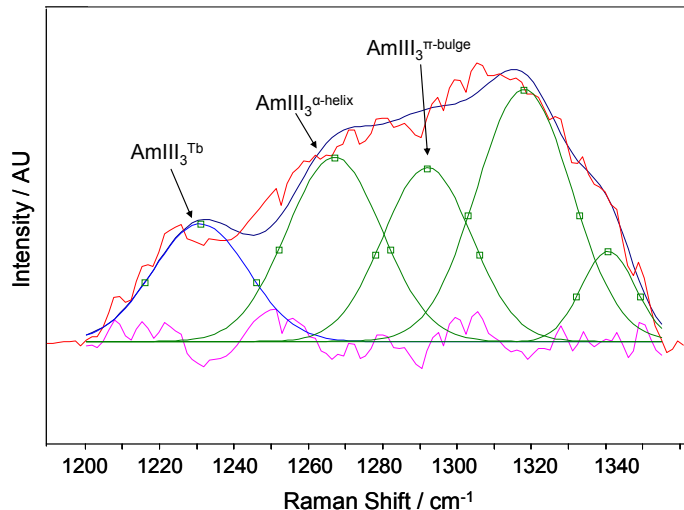


Figure S7. Deconvolution of the AmIII region from the non-PPII part of the spectrum for the mutant peptide as the sum of five Gaussians. Fit statistics: reduced $\chi^2 = 13.673$; $R^2 = 1.0301$; standard error = 29.8235.

References

- (1) Mikhonin, A. V.; Asher, S. A.; Bykov, S. V.; Murza, A. *J. Phys. Chem. B* **2007**, *111*, 3280.
- (2) Zondlo, S.; Lee, A.; Zondlo, N. *Biochemistry* **2006**, *45*, 11945.
- (3) Ma, L.; Ahmed, Z.; Mikhonin, A. V.; Asher, S. A. *J. Phys. Chem. B* **2007**, *111*, 7675.
- (4) Asher, S.; Mikhonin, A.; Bykov, S. *J. Am. Chem. Soc.* **2004**, *126*, 8433.
- (5) Mikhonin, A. V.; Bykov, S. V.; Myshakina, N. S.; Asher, S. A. *J. Phys. Chem. B* **2006**, *110*, 1928.
- (6) Mikhonin, A. V.; Asher, S. A. *J. Am. Chem. Soc.* **2006**, *128*, 13789.
- (7) Mikhonin, A. V.; Myshakina, N. S.; Bykov, S. V.; Asher, S. A. *J. Am. Chem. Soc.* **2005**, *127*, 7712.
- (8) Ding, F.; Prutzman, K. C.; Campbell, S. L.; Dokholyan, N. V. *Structure* **2006**, *14*, 5.
- (9) Ahmed, Z.; Myshakina, N. S.; Asher, S. A. *J. Phys. Chem. B* **2009**, *113*, 11252.
- (10) Xiong, K.; Asher, S. A. *Biochemistry* **2010**, *49*, 3336.
- (11) Xiong, K.; Ascutto, E. K.; Madura, J. D.; Asher, S. A. *Biochemistry* **2009**, *48*, 10818.